

# Barrier Mediated Predator-Prey Dynamics under Periodic Boundary Conditions

Bachelor Thesis

submitted by

**Jessica Wonges**

Institute of Theoretical Physics II: Soft Matter  
Faculty of Mathematics and Natural Sciences  
Heinrich-Heine-University Düsseldorf

5th May 2023

Supervisor: Prof. Dr. Harmut Löwen  
Co-Supervisor: Prof. Dr. Jürgen Horbach  
Additional Advisors: Paul Monderkamp, Dr. Fabian Schwarzendahl



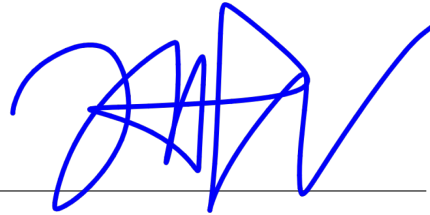
## Declaration of Authorship

I hereby certify that the thesis submitted is the result of my own research and that I have not used any references or resources other than those stated. I also confirm that this work has not previously been submitted to any other academic examination or assessment.

Düsseldorf, 5th May 2023

---

Place, Date

A handwritten signature in blue ink, consisting of a series of loops and a long horizontal stroke, positioned above a horizontal line.

Jessica Wonges



## Abstract

Predator-prey dynamics are crucial for the survival of an ecosystem. The likelihood of a prey being caught by a predator depends not only on their relative speeds but also on the characteristics of their local environment. For example, in the macroscopic world, the wolf must be able to move through a dense forest in order to catch the deer. In this study, we introduce an idealised one-dimensional model in which a prey and a predator must overcome a potential barrier to engage in a chase. The model is based on the overdamped Newtonian equation, and it is solved for two possible cases: on a parabolic potential barrier and on a periodic potential barrier.

To determine the likelihood of a predator catching the prey, it is necessary to understand the timing and location of catching events. Therefore, we introduce methods on finding the catching time and position. It is not possible to solve this analytically, therefore we need numerical solutions through simulations.

Within the parabolic potential barrier, catching and escape can occur. In the periodic potential barrier, however, escape is undefined. Therefore, we study the behaviour of the predator and prey in a periodic potential barrier as they chase each other in a circular trajectory. We investigate the number of revolutions required for the predator to catch the prey and discuss our findings.



# Contents

<b>1</b>	<b>Introduction</b>	<b>1</b>
<b>2</b>	<b>Methods</b>	<b>3</b>
2.1	The ideal predator-prey model . . . . .	3
2.1.1	Parabolic Predator-Prey Potential . . . . .	3
2.1.2	Periodic Predator-Prey Potential . . . . .	4
2.2	Analytical solutions . . . . .	6
2.2.1	Parabolic potential . . . . .	6
2.2.2	Periodical potential . . . . .	7
2.3	Catching time and position . . . . .	8
2.3.1	Catching time and position for parabolic boundary condition . . . . .	8
2.3.2	Catching time and position for the periodical boundary condition . . . . .	9
<b>3</b>	<b>Linear predator-prey results</b>	<b>12</b>
3.1	Trajectory . . . . .	12
3.2	Catching time . . . . .	15
3.3	Catching position . . . . .	16
3.4	Regions . . . . .	20
<b>4</b>	<b>Periodic predator-prey results</b>	<b>21</b>
4.1	Trajectory . . . . .	21
4.2	Catching time . . . . .	22
4.3	Catching revolutions . . . . .	26
<b>5</b>	<b>Summary and Outlook</b>	<b>29</b>







# 1 Introduction

The ability to find food and avoid danger is vital to the survival of any animal. While a predator must catch its prey in order to meet its nutritional needs and survive, the prey seeks to evade the predator's clutches in order to ensure its own survival. Among the many factors that contribute to this feat, the speed of both predator and prey plays a critical role in determining the outcome of a catching. [1] The general rule is that catching occurs when the predator is faster than the prey, while an escape happens if the prey is swifter. [2]

In an inhomogeneous landscape, however, the situation is much more complex. For example, an inhomogeneous landscape can include areas of dense forest, open grassland, rocky outcrops and bodies of water such as rivers or lakes. Therefore, the local speed, which describes the speed at which prey and predators move through the habitat, depends on the details of the environment and this influences the outcome of the catching. [3, 4]

One of the many cases in nature is the macroscopic example of the wolf and the deer. A rich forest with rivers would make it harder for the wolf to hunt the deer, because the deer will have no problem crossing a river, but the wolf might have to swim slowly to reach the other side. The obstacle affects both the predator and the prey in different ways, ultimately determining the outcome of the chase. It may even make it impossible for the wolf to catch the deer, making this hunt an unfavourable strategy for survival in this particular case. [5, 6]

White blood cells and pathogens are another example of microscopic predator-prey dynamics as they seek out and eliminate the pathogens in biological organisms such as the human body. Pathogens can infect different parts of the human body, and white blood cells travel through the lymphatic system to find the site of infection. [7] In addition, microswimmers generally face different types of obstacles in their environment depending on their swimming strategies, such as pushers or pullers, and their species. [8, 9] Further microscopic examples of the predator-prey dynamics have also been artificially created through experiments, such as oil droplets following each other. The unanimated prey-predator system is experimentally expected to have similar dynamics with our one-dimensional model. The droplets are designed to use synthetic colloidal particles that are confined in a microfluidic channel. They interact in a non-reciprocal way, which means they are able to chase each other in a one directional setting. [10, 11]

In this thesis, we discuss a general theoretical analysis of this type of predator-prey dynamics. Specifically, we study systems of two particles, each of which has its own self-propelled velocity, moving in environments that are modelled as potential landscapes, so they also have coupling constants respective to the potential barrier, and they interact with the potential barrier differently. One particle acts as prey and the other as predator, with different starting points on the potential. The equation is based on the overdamped Newtonian equation of motion without noise, and this is solved exactly in two cases: one on a potential hill and on a periodic potential.

The thesis is structured as follows. In Sec.(2.1)-(2.2), we introduce the idealised model of the predator-prey dynamics and followed by a breakdown of the Newtonian equation of motion to model the potential barrier for both parabolic and periodic boundary conditions. In Sec.(2.3), we explain the methods on how to find the time and position, where the predator catches the prey, or it escapes and followed by a throughout discussion of the results for both parabolic and periodic boundary conditions, which concludes the trajectories of both prey and predator, the catching time and position related to their self-propulsion velocity and coupling constants in Sec.(3)-(4). Additionally, in Sec.(4.3) we also discuss the number of revolutions needed for the prey to catch the predator in a periodic boundary setting.

## 2 Methods

### 2.1 The ideal predator-prey model

An idealised model of both prey and predator is proposed here using a one-dimensional model, which serves as a proof of principle for more complicated frameworks, that can classify different characteristic states for both catching and escaping when faced with an obstacle. Our starting point is Newton's equation, which reads as follows

$$m \frac{d\mathbf{u}(t)}{dt} = -\gamma \mathbf{u}(t) + \gamma v_0 \mathbf{e} + \mathbf{F}(\mathbf{r}, t). \quad (1)$$

As the particle moves through an inhomogeneous landscape, friction between particle and environment can occur. This friction model is represented by  $-\gamma \mathbf{u}(t)$ , where  $\gamma$  is the coefficient of friction and  $\mathbf{u}(t)$  is the velocity of the particle as a function of time. The term  $\gamma v_0 \mathbf{e}$ , describes the self-propulsion velocity  $v_0$  along the particle's orientation  $\mathbf{e}$ . Furthermore,  $m$  is the mass of the particle,  $\mathbf{r}$  is its position and  $\mathbf{F}(\mathbf{r}, t)$  is an external force. The Reynolds number  $Re = \frac{\rho U L}{\mu}$  [12, 13], which compares the inertial and viscous effects, is relatively low for micron-sized objects such as colloids, bacteria or microalgae [14]. Therefore, the left-hand inertial term in Eq.(1) can be neglected. The equation simplifies to

$$\mathbf{u}(t) = v_0 \mathbf{e} + \frac{1}{\gamma} \mathbf{F}(\mathbf{r}, t), \quad (2)$$

which is an overdamped equation of motion. To understand the model further, we first consider the parabolic potential, which is shown in the following section.

#### 2.1.1 Parabolic Predator-Prey Potential

Now we model the motion of a predator and a prey using Eq.(2), where both are subjected to a barrier. This is modelled by the external force  $\frac{1}{\gamma} \mathbf{F}(\mathbf{r}, t)$  in Eq.(2) is given by  $\alpha_i x_i$  in the Eq.(4)-(5), which is the gradient of a potential  $F_i = -\nabla U_i$  of a parabolic form, that is

$$U_i(x) = -\frac{1}{2} \alpha_i x_i^2. \quad (3)$$

Explicitly in one dimension, Eq.(2) simplifies to

$$\dot{x}_1 = v_1 + \alpha_1 x_1, \quad (4)$$

$$\dot{x}_2 = v_2 + \alpha_2 x_2, \quad (5)$$

for the position of the prey  $x_1$  and the predator  $x_2$ , respectively. Here,  $v_1$  and  $v_2$  are the self-propulsion velocities and  $\alpha_i$  are coupling constants to the respective potential barrier. A schematic of the potential barrier is shown in Fig.(1).

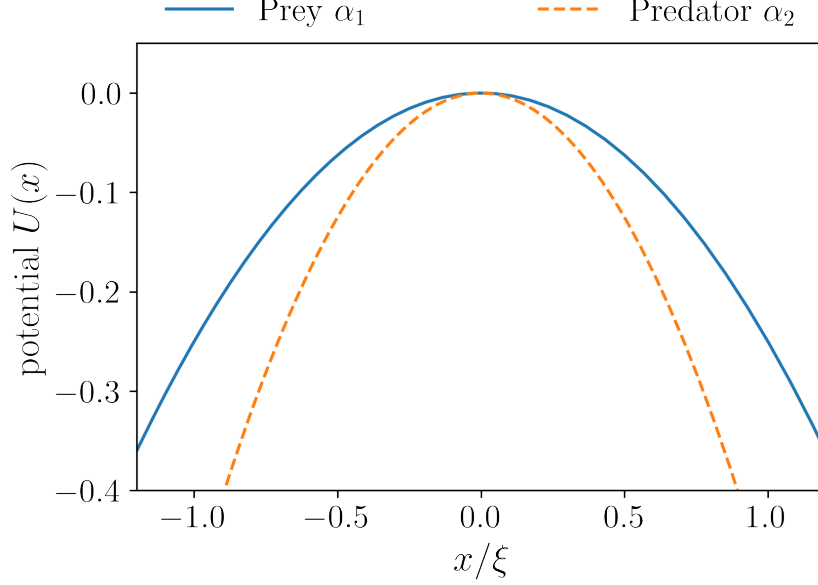


Figure 1: Potentials of the prey and the predator in parabolic form according to their positions  $x/\xi$ , with their respective coupling constants  $\alpha_1 = 0.5$ ,  $\alpha_2 = 2$ .

### 2.1.2 Periodic Predator-Prey Potential

Since catching and escape are observed based on the ability of prey and predator to overcome the potential barrier, the possibility of a circular potential barrier is considered. Therefore, the closest observation of a circular motion would be a periodic barrier within a specific range. The analysis in Sec.(2.1) also applies here. The periodic potential is given by

$$U_i(x) = -\alpha_i \cdot (1 + \cos x_i). \quad (6)$$

with the constraint  $U(0) = U(2\pi)$ . So the potential loops between 0 and  $2\pi$  to represent a circular motion. The external force in Eq.(2) is now changed to a periodic function  $\alpha_i \sin x_i$  based on  $F_i = -\nabla U_i$ . Therefore, position of the prey and predator can be described as

$$\dot{x}_1 = v_1 - \alpha_1 \sin x_1, \quad (7)$$

$$\dot{x}_2 = v_2 - \alpha_2 \sin x_2, \quad (8)$$

where again  $v_i$  with  $i = 1, 2$  describes the self-propulsion velocity and  $\alpha_i$  the coupling constants to the respective potential barrier. A schematic of the periodic potential barrier is shown in Fig.(2)

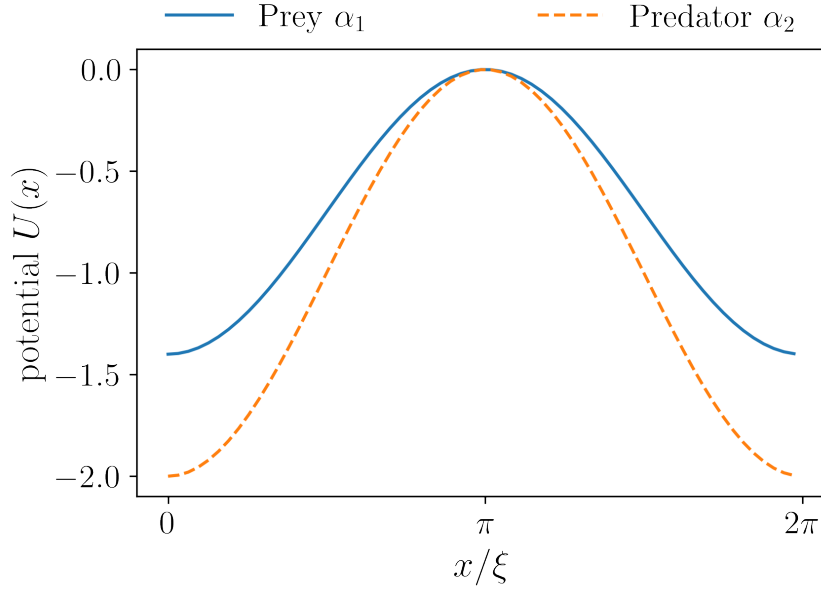


Figure 2: Potentials of the prey and the predator in periodic form according to their positions  $x/\xi$ , with their respective coupling constants  $\alpha_1 = 0.7$ ,  $\alpha_2 = 1$ .

## 2.2 Analytical solutions

### 2.2.1 Parabolic potential

To determine the positions  $x_i$  with  $i = 1, 2$  of the prey and predator, we analytically solve the linear differential equations Eq.(4)-(5). The equations are first-order equations with variable coefficients. Therefore, these are the steps that are used to find  $x(t)$ :

1. The first step is to rewrite the equation into a homogeneous equation. Here we can assume that  $v_i = 0$  and  $\dot{x}_i = \alpha_i x_i$ . Integration gives:

$$\begin{aligned}\int \frac{1}{x_i} dx_i &= \int \alpha_i dt, \\ \ln x_i &= \alpha_i t + c_i, \\ x_i &= e^{\alpha_i t + c_i} = \tilde{C} \cdot e^{\alpha_i t}.\end{aligned}$$

Thus, the general solution of the homogenous equation is

$$x_{i,hom}(t) = \tilde{C} \cdot e^{\alpha_i t}. \quad (9)$$

2. We can determine the special solution of the non-homogenous equation by assuming that  $x_{i,sp}(t) = \tilde{C}(t) \cdot e^{\alpha_i t}$ . The first derivative of this equation is equal to the original equation. As a result, the function  $\tilde{C}(t)$  can be calculated by

$$\dot{x}_i(t) = \dot{\tilde{C}}(t) \cdot e^{\alpha_i t} + \alpha_i \tilde{C}(t) \cdot e^{\alpha_i t} \stackrel{!}{=} v_i + \alpha_i x_i.$$

The result from Eq.(9) gives

$$\begin{aligned}\dot{\tilde{C}}(t) \cdot e^{\alpha_i t} + \cancel{\alpha_i \tilde{C}(t) \cdot e^{\alpha_i t}} &= v_i + \cancel{\alpha_i \tilde{C}(t) \cdot e^{\alpha_i t}} \\ \tilde{C}(t) &= v_i \int e^{-\alpha_i t} dt = -\frac{v_i}{\alpha_i} \cdot e^{-\alpha_i t},\end{aligned}$$

which yields the special solution

$$x_{i,sp}(t) = \tilde{C}(t) \cdot e^{\alpha_i t} = -\frac{v_i}{\alpha_i} \cdot e^{-\alpha_i t} \cdot e^{\alpha_i t} = -\frac{v_i}{\alpha_i}. \quad (10)$$

3. Therefore, the general solutions to the non-homogeneous equation is the sum of the solution from Eq.(9) and Eq.(10), which reads

$$x_i(t) = \tilde{C} \cdot e^{\alpha_i t} - \frac{v_i}{\alpha_i} = \frac{1}{\alpha_i} \left( \alpha_i \cdot \tilde{C} \cdot e^{\alpha_i t} - v_i \right). \quad (11)$$

4. The initial condition  $x(0) = \frac{1}{\alpha_i}(\alpha_i \cdot \tilde{C} - v_i)$  is required to be fulfilled in this equation, that is

$$\tilde{C} = \frac{1}{\alpha_i}(v_i + \alpha_i x_i(0)).$$

We arrive at the full solution to the Eq(4)-(5) for both prey and predator

$$x_1(t) = \frac{1}{\alpha_1}((v_1 + \alpha_1 x_1(0))e^{\alpha_1 t} - v_1), \quad (12)$$

$$x_2(t) = \frac{1}{\alpha_2}((v_2 + \alpha_2 x_2(0))e^{\alpha_2 t} - v_2). \quad (13)$$

### 2.2.2 Periodical potential

We now solve the non-linear differential equations Eq.(7)-(8) of the periodical potential analogue to the steps in Sec.(2.2). This gives

$$x_1(t) = 2 \cdot \arctan \left( \frac{\alpha_1 - \sqrt{v_1^2 - \alpha_1^2} \cdot \tan \left( -\frac{1}{2}t\sqrt{v_1^2 - \alpha_1^2} - \arctan \frac{-\alpha_1\sqrt{v_1^2 - \alpha_1^2} + v_1\sqrt{v_1^2 - \alpha_1^2} \cdot \tan \left( \frac{x_1}{2} \right)}{v_1^2 - \alpha_1^2} \right)}{v_1} \right), \quad (14)$$

$$x_2(t) = 2 \cdot \arctan \left( \frac{\alpha_2 - \sqrt{v_2^2 - \alpha_2^2} \cdot \tan \left( -\frac{1}{2}t\sqrt{v_2^2 - \alpha_2^2} - \arctan \frac{-\alpha_2\sqrt{v_2^2 - \alpha_2^2} + v_2\sqrt{v_2^2 - \alpha_2^2} \cdot \tan \left( \frac{x_2}{2} \right)}{v_2^2 - \alpha_2^2} \right)}{v_2} \right). \quad (15)$$



## 2.3 Catching time and position

To determine whether the predator has caught the prey or not, we need to be able to determine the time and position of the catch. The catching time  $t^*$  is determined by the condition

$$x_1(t^*) = x_2(t^*), \quad (16)$$

which gives us also the catching position  $x^* = x_{1,2}(t^*)$ . In the following, we define  $\tau = 1/\alpha_2$  as a natural unit of time and  $\xi = v_2/\alpha_2 = v_2\tau$  a natural length scale. These represent the physical time and length scales related to the predator.

### 2.3.1 Catching time and position for parabolic boundary condition

Although we have solved Eqs.(4)-(5) as shown in Sec.(2.2), it is not possible to solve analytically the catching condition Eq.(16). Therefore, we evaluate Eq.(16) numerically using Halley's method. Halley's method is the second class of Householder's method, a root-finding algorithm, which is a higher order of Newton's method. With Halley's method, we can find better approximations to the roots of Eq.(16), which gives us the catching time. The basic idea of the method is to use an initial guess  $x_{n=0}$  for the root of the Eq. (17) and then iteratively refine the guess to find the next value  $x_{(n=0)+1} = x_1$  until the desired level of accuracy is achieved. We use the following formula from [15] to calculate the next guess for the root:

$$x_{n+1} = x_n - \frac{2f(x_n)f'(x_n)}{2[f'(x_n)]^2 - f(x_n)f''(x_n)}. \quad (17)$$

$f(x)$  is the function whose root we are looking for,  $f'(x)$  is the first derivative of the function and  $f''(x)$  is the second derivative. The iteration is performed until the value of  $x_n$  in the function  $f(x)$  is approximately zero. The formula used in Eq.(17) is derived using Taylor series expansion of  $f(x)$ . This allows us to approximate the root of a function using a polynomial of higher degree. It takes into account the curvature of the function by using the second derivative, which can lead to faster convergence. [16] Therefore, the first and second derivative of Eq.(4)-(5) are

$$\dot{x}_i(t) = (v_i + \alpha_i x(0))e^{\alpha_i t}, \quad (18)$$

$$\ddot{x}_i(t) = \alpha_i(v_i + \alpha_i x(0))e^{\alpha_i t}. \quad (19)$$

The knowledge of the catching time and position for the parabolic boundary condition allows us to classify five different catching cases and five different escaping cases by considering the

initial conditions and the long time limits of Eq.(12)-(13), which are summarised in Table (1) and Table (2).

case	description	initial conditions	catching condition
Ca. I	caught while summiting the barrier	$x_1(0) < 0, x_2(0) < x_1(0)$	$x^* > x_1(0)$
Ca. II	caught after summiting the barrier	$x_1(0) < 0, x_2(0) < x_1(0)$	$x^* > 0$
Ca. III	caught after prey summits	$x_1(0) > 0, x_2(0) \geq 0$	$x^* > 0$
Ca. IV	caught descending the barrier	$x_1(0) > 0, x_2(0) \leq 0$	$x^* > 0$
Ca. V	caught descending the barrier without summiting	$x_1(0) < 0, x_2(0) < x_1(0)$	$x^* < x_1(0)$
Es. I	both are summiting the barrier	$x_1(0) < 0, x_2(0) < x_1(0)$	$x_1(\infty) = x_2(\infty) = \infty$
Es. II	both descending in positive direction	$x_1(0) > 0, 0 < x_2(0) < x_1(0)$	$x_1(\infty) = x_2(\infty) = \infty$
Es. III	both descending in opposite directions	$x_1(0) > 0, x_2(0) < 0$	$x_1(\infty) = \infty, x_2(\infty) = -\infty$
Es. IV	both descending in negative directions	$x_1(0) < 0, x_2(0) < x_1(0)$	$x_1(\infty) = x_2(\infty) = -\infty$
Es. V	only prey is summiting the barrier	$x_1(0) < 0, x_2(0) < 0$	$x_1(\infty) = \infty, x_2(\infty) = -\infty$

Table 1: Classification of catching and escape scenarios determined by initial conditions and catching conditions. [17]

initial condition $x_1$	initial condition $x_2$	cases	
		catching	escape
$x_1(0) = -\xi/3$	$x_2(0) = -\xi/2$	I, II, V	I
$x_1(0) = -\xi/3$	$x_2(0) = -3\xi/2$	V	V, IV
$x_1(0) = \xi/4$	$x_2(0) = -\xi/4$	III	III
$x_1(0) = \xi/2$	$x_2(0) = \xi/4$	IV	II

Table 2: Initial conditions for different catching and escape cases.

### 2.3.2 Catching time and position for the periodical boundary condition

In the periodic boundary condition, the prey and predator can cross not just once, but several times over a period of time, which is shown in Fig.(3). However, we are only interested in the first intersection of the two trajectories and define this as a catching. In Fig.(4) shows the position difference between the prey and the predator, when we insert Eqs.(14)-(15) in the condition Eq.(16). The resulting function  $x(t) = x_1(t) - x_2(t)$  is discontinuous and its values jump from positive to negative and vice versa on several occasions. The function also shows discontinuity in it's second derivative. Therefore, it's not possible to use the Haley's method to find the accurate

value for this function's roots, which requires a continuous second derivative. [15, 16]

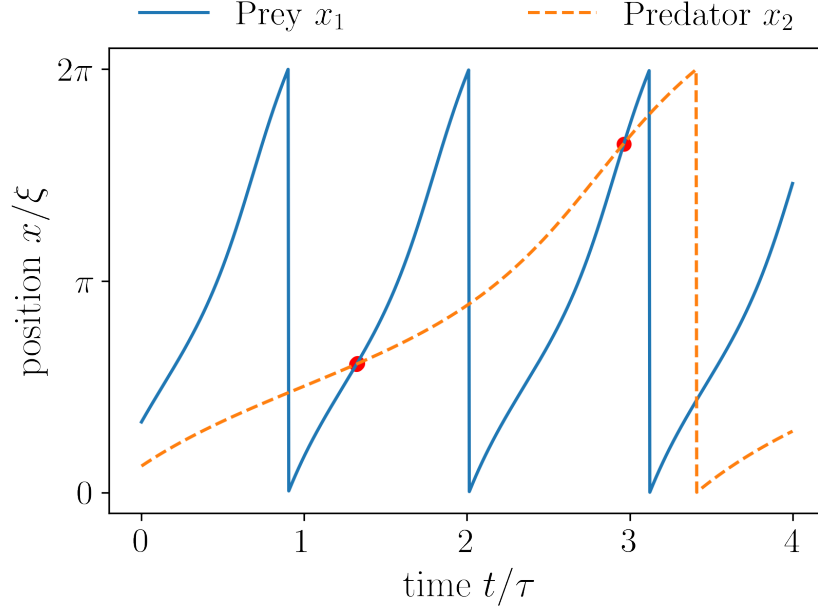


Figure 3: Periodic predator-prey trajectory with the conditions  $x_1(0) = \pi\xi/3$  and  $x_2(0) = \pi\xi/8$ . The red dots show where the prey and the predator cross each other.

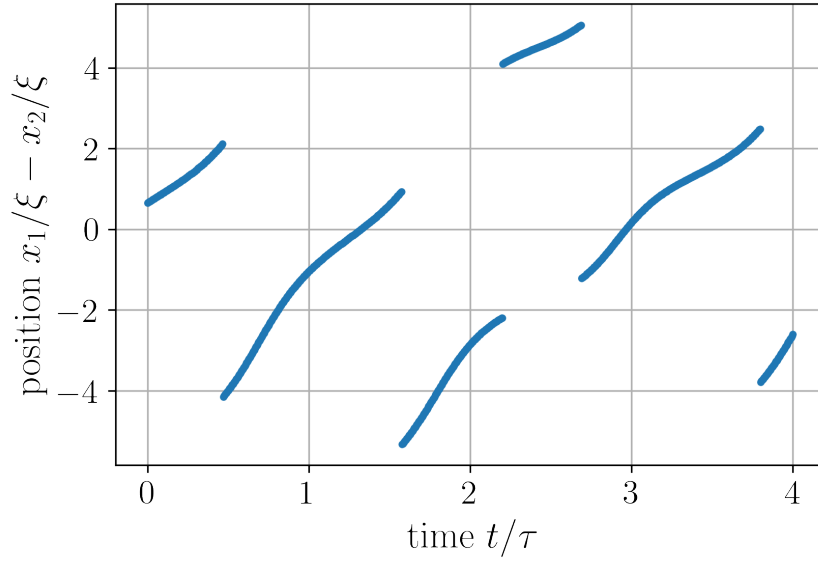


Figure 4: Position difference of Eqs.(14)-(15) when plotted with the condition in Eq.(16), with the initial conditions  $x_1(t) = \pi\xi/3$  and  $x_2(0) = \pi\xi/8$

Therefore, we use a different approach to find the catching time for the periodic boundary

condition by defining the catching time  $t^*$  when the position difference is as close to zero as possible.

$$|x_1(t^*) - x_2(t^*)| \approx 0 \quad (20)$$

This also gives us the catching position  $x^* = x_{1,2}(t^*)$ . With this information, we can determine the number of revolutions needed for a successful catching. First, we look at the distance travelled by the prey, shown as the green line in Fig.(5). Since we already know the catching time  $t^*$ , we can look for the distance travelled until the catching occurred, this is shown as the red dot. Then we divide the value by  $2\pi$  and round the result up to the nearest integer to determine the number of revolutions required for the catch to occur. As an example, in the Fig.(5) shows that after the prey has looped the potential three times, the predator is able to catch the prey. This information is crucial to discuss the results later in Sec.(4.3).

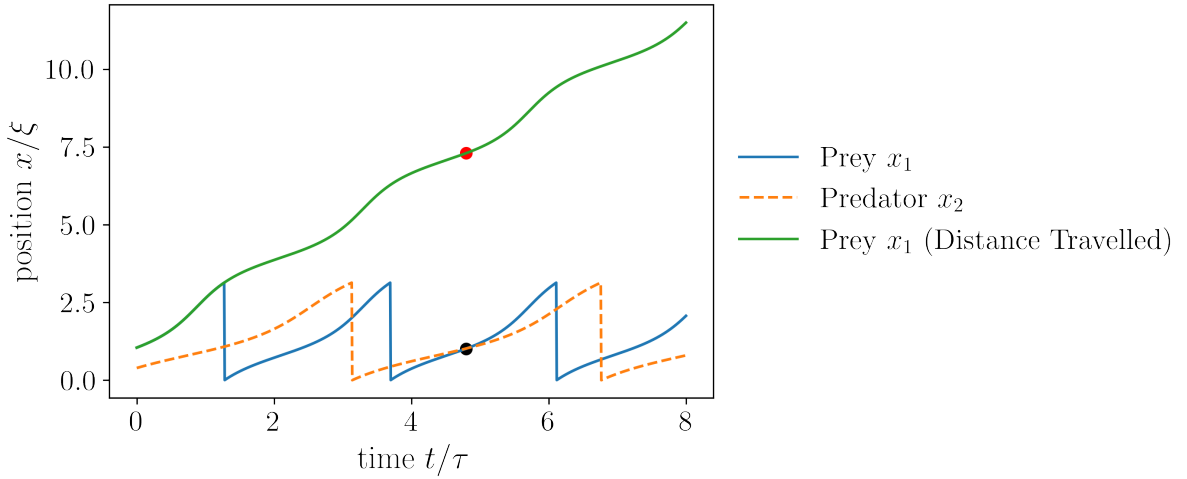


Figure 5: Periodic predator-prey positions with the condition  $x_1(0) = \pi\xi/3$  and  $x_2(0) = \pi\xi/8$ . The green line shows the distance travelled by the prey, and the red dot represents the final position of catching.

### 3 Linear predator-prey results

In this section, we will concentrate on catching and escaping cases with the initial conditions  $x_1(0) = -\xi/3$ ,  $x_2(0) = -\xi/2$ , as shown in Table (3).

case	description	catching condition
Ca. I	caught while summiting the barrier	$x^* > x_1(0)$
Ca. II	caught after summiting the barrier	$x^* > 0$
Ca. V	caught descending the barrier without summiting	$x^* < x_1(0)$
Es. I	both are summiting the barrier	$x_1(\infty) = x_2(\infty) = \infty$

Table 3: Catching and escape with the initial condition  $x_1(0) = -\xi/3$ ,  $x_2(0) = -\xi/2$

With different parameters of velocity  $v_i$  and alpha  $\alpha_i$ , respectively to the time, the outcome of the catching differs greatly and, in some cases, the prey manages to escape. To make things easier in the calculation, we fixate the predator's velocity  $v_2$  and alpha  $\alpha_2$  as 1, which gives  $\xi = v_2/\alpha_2 = 1$ . However, we use a range of parameters for the prey's velocity and its coupling constant.

#### 3.1 Trajectory

The Figs.(6)-(9) in this section show the position of the prey and predator  $x/\xi$  respectively by the time  $t$ . The sub-figures are classified based on their initial condition, as shown in Table (2). The parameters  $v_1$  and  $\alpha_1$  are changed accordingly to the specific regions following the Table (1) to show at which time the predator catches the prey. If the predator catches the prey, they will meet at a specific time, and this event is marked by the black dot. If the Eq.(12) and Eq.(13) from the initial time  $t = 0$  does not cross each other, the prey has escaped the predator and no catching occurs.

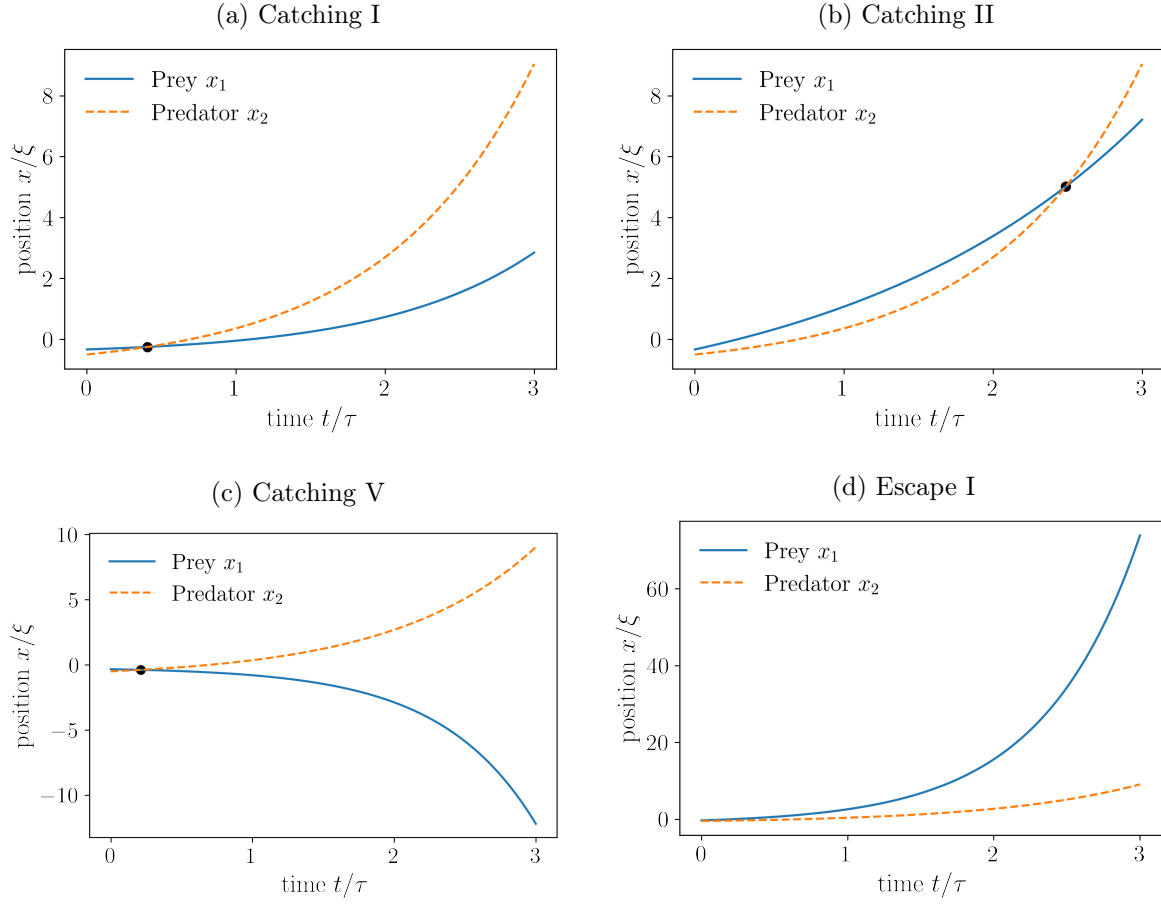


Figure 6: Predator-prey positions in with the condition  $x_1(0) = -\xi/3$  and  $x_2(0) = -\xi/2$ . The black dot marks the catching event.

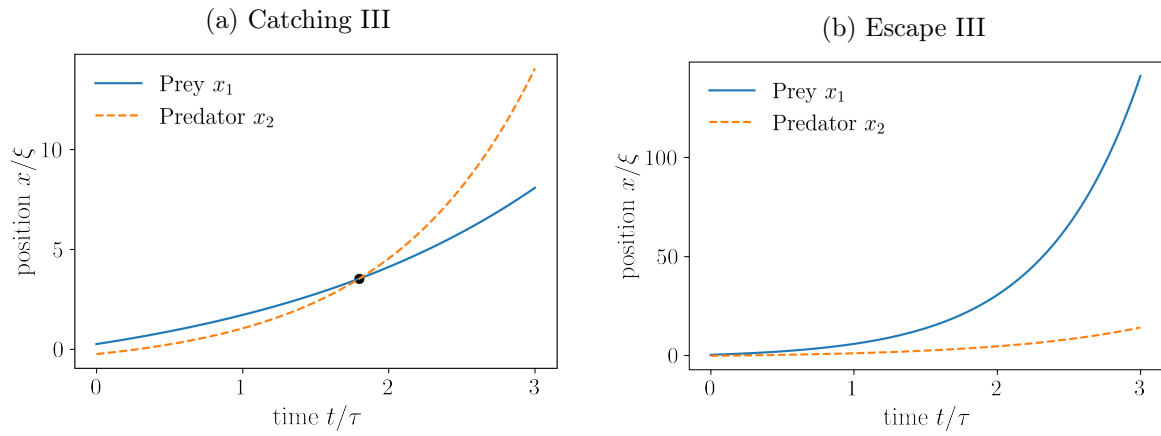


Figure 7: Predator-prey positions in with the condition  $x_1(0) = \xi/4$  and  $x_2(0) = -\xi/4$ . The black dot marks the catching event.

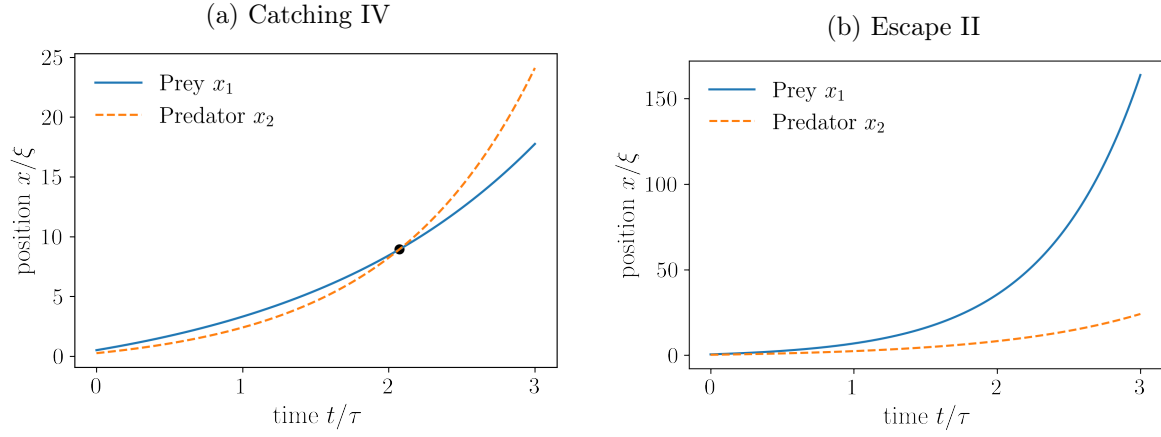


Figure 8: Predator-prey positions with the condition  $x_1(0) = \xi/2$  and  $x_2(0) = \xi/4$ . The black dot marks the catching event.

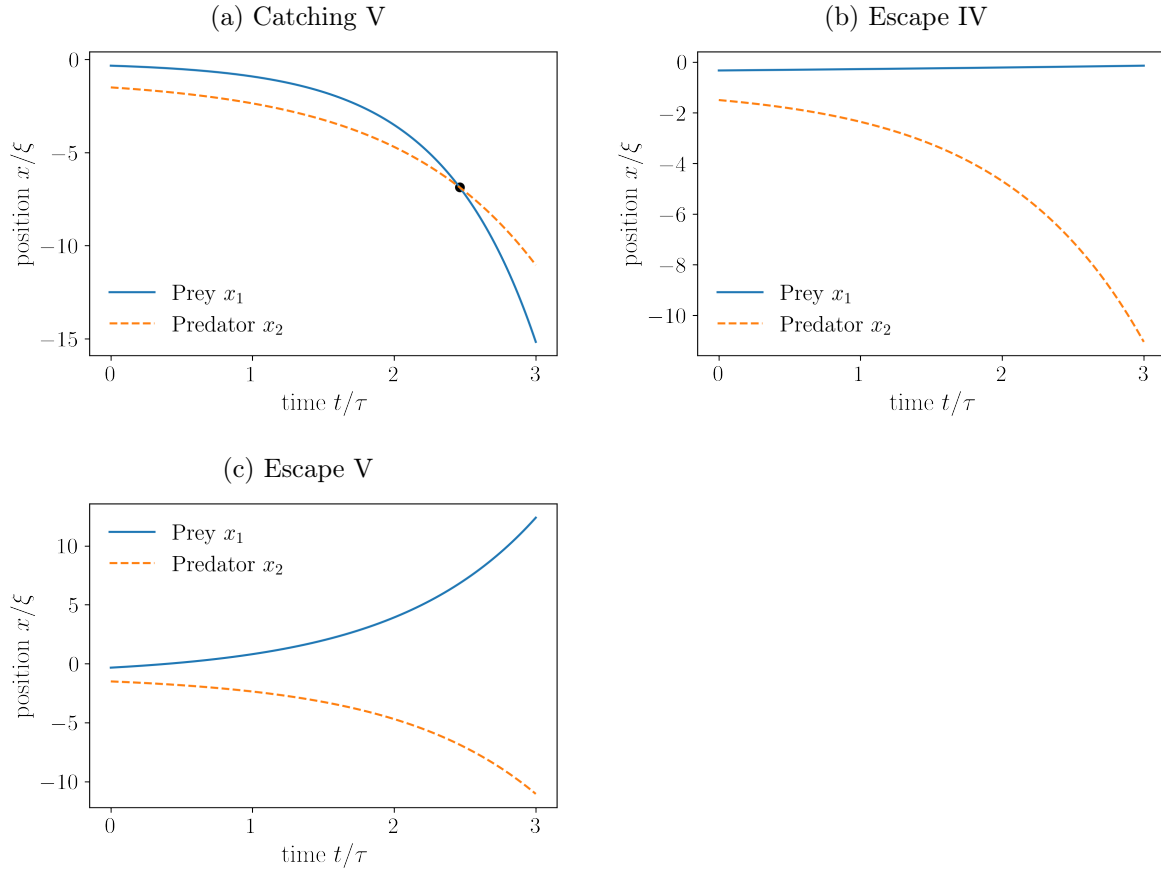


Figure 9: Predator-prey positions with the condition  $x_1(0) = -\xi/3$  and  $x_2(0) = -3\xi/2$ . The black dot marks the catching event.

### 3.2 Catching time

We now examine the catching time determined by Eq.(17) for different coupling constants and self-propulsion velocity.

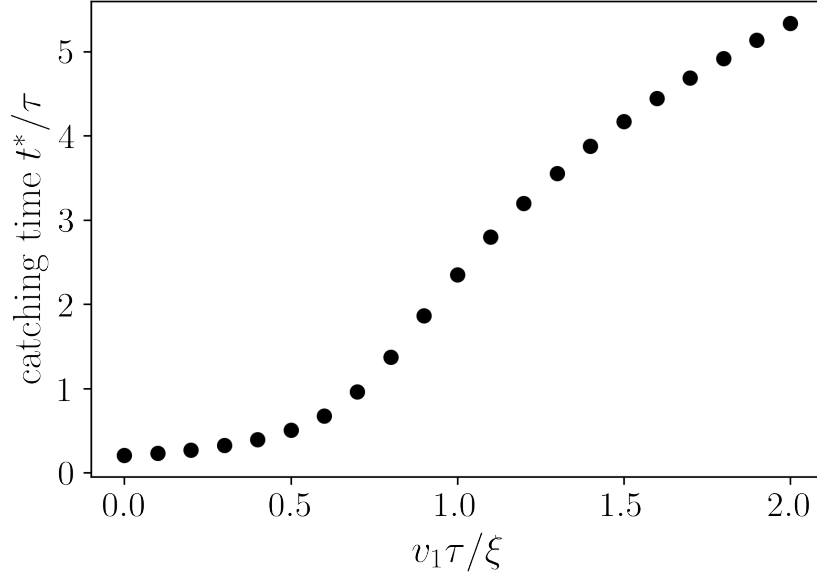


Figure 10: Catching time of prey and predator respectively to its self-propulsion velocities, where  $\alpha_1 < \alpha_2$

Fig.(10) shows the catching time, when the prey has a smaller coupling constant than the predator  $\alpha_1 < \alpha_2$  with a wide range of self-propulsion velocity, where the prey is slower  $v_1 < v_2$  or faster  $v_1 > v_2$  than the predator. The small coupling constant  $\alpha_1$  value ensures that the prey will definitely be caught by the predator. The first few values of the self-propulsion velocity, when the prey is slower than the predator  $v_1 < v_2$ , show that catching occurs much faster. When the prey's self-propulsion velocity increases, it also increases the catching time since the predator needs to catch up to the prey.



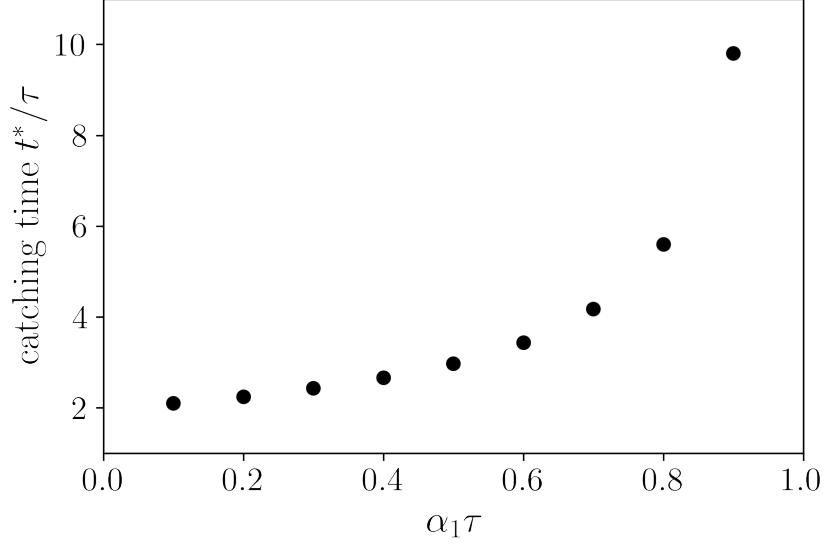


Figure 11: Catching times of prey and predator, respectively to its coupling constants, where  $v_1 > v_2$

Fig.(11) shows the catching time, when we approach the coupling constant  $\alpha_1 \rightarrow \alpha_2$ , where the prey is faster than the predator  $v_1 > v_2$ . Catching occurs much faster with smaller coupling constant values, but only when  $\alpha_1 < \alpha_2$ , because the catching time begins to diverge at  $\alpha_1 = \alpha_2 = \alpha$ . An approximation of the solution Eq.(4)-(5) for barrier dominated motion is used to understand the scaling of this divergence, which according to [17] yields the catching time

$$t^* \sim 1/(\alpha_1 - \alpha_2). \quad (21)$$

For  $\alpha_1 > \alpha_2$ , the self-propulsion velocity of the predator is not sufficient any more to catch the prey since the motion of both predator and prey is dominated by them descending the barrier. As we get closer to the divergence, the catching dynamics are dominated by the potential barrier, and the importance of self-propulsion decreases. After  $\alpha_1 > \alpha_2$  the predator cannot catch up to the prey, so the prey is able to escape.

### 3.3 Catching position

Every catching happens at a certain position around the barrier. Using the numerically calculated catching time, we can find the position of a catching. In this section, we can see through the figures that at a certain coupling constant value and velocity, where the catching happens. To see the position of the prey and predator, we compare Figs.(12)-(15) to Fig.(1) which shows

the catching position on the potential barrier. A negative value represents a catching that occurs before the summit ( $x^* = 0$ ), while a positive value represents a catching that occurs after the summit.

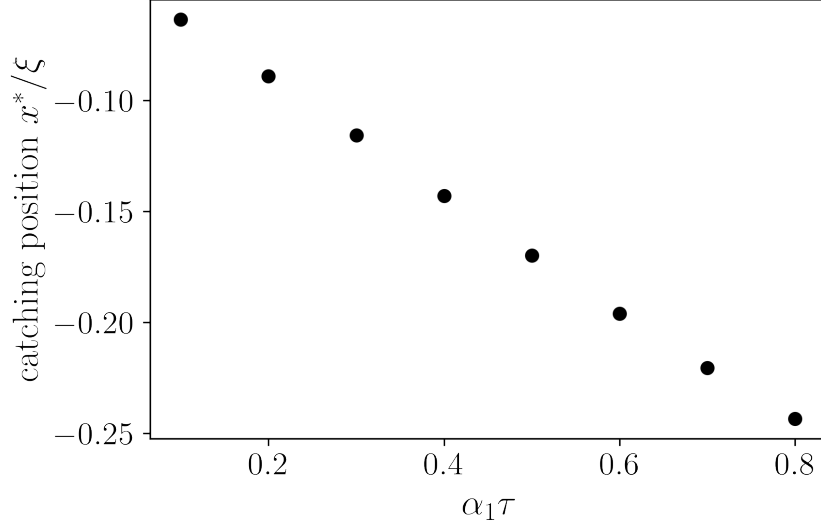


Figure 12: Catching I with increasing values of coupling constants, respectively to its catching positions and  $v_1 < v_2$

The self-propulsion velocity and the coupling constant of the prey is smaller than the predator in the following Fig.(12)-(13). The catching position decreases with increasing coupling constants, as shown in Fig.(12). Furthermore, each catching happens before the initial position of the prey ( $x^* > x_1(0)$ ). This means that the catching happens while the prey is moving towards the summit. The first catching with the smallest coupling constant happens long after the prey almost reaches the summit, and the last catching with the biggest coupling constant happens near the initial position. This catching is classified as Catching I.

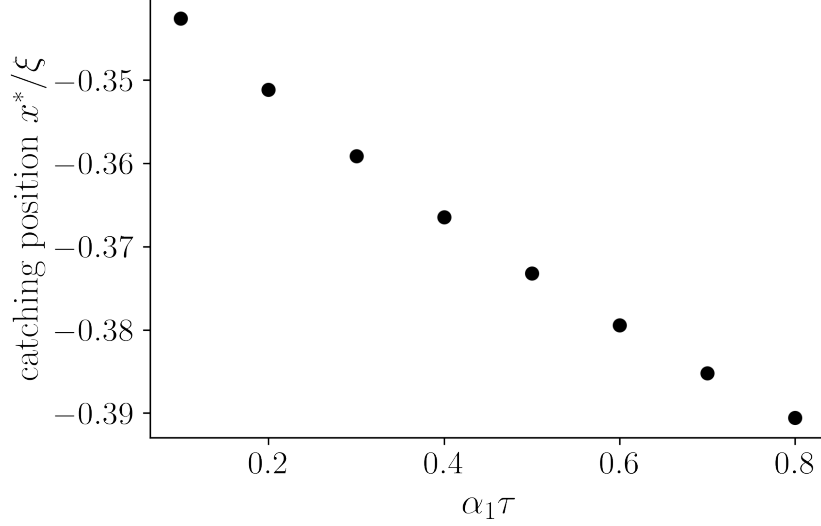


Figure 13: Catching V with increasing values of coupling constants, respectively to its catching position and  $v_1 < v_2$

Fig.(13) shows that the catching position also decreases with increasing coupling constants. However, all catching occurs for values  $x^* < x_1(0)$ . The prey is therefore caught while moving away from the summit in the negative x-direction. The first catching in the figure happens not far from the initial position, with a small coupling constant. This catching is classified into Catching V.

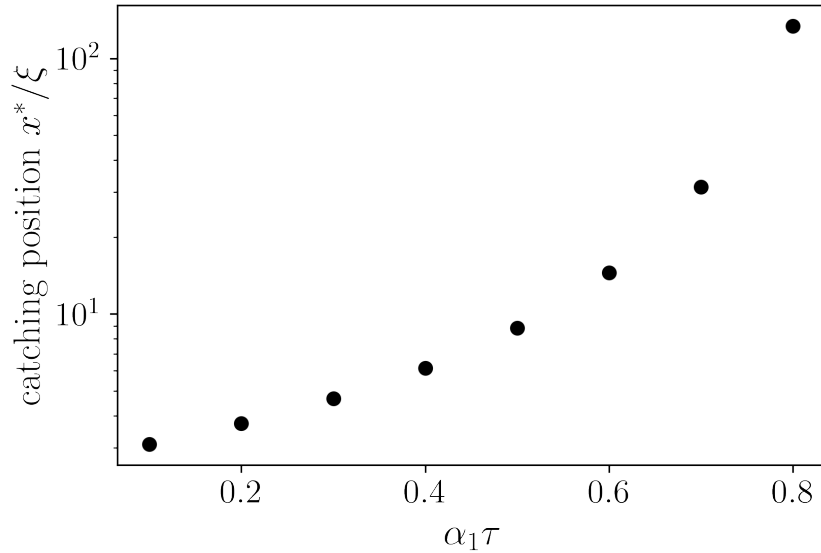


Figure 14: Catching II with increasing values of coupling constants, respectively to its position and  $v_1 > v_2$

We can see, however, that in the Fig.(14), all the catching has a positive value. This shows that all catching happens after the summit. Here, the self-propulsion velocity of the prey is higher than the predator, but its coupling constant is still smaller. This is referred to as Catching II. Similar to the explanation in in (3.2), when the prey reaches an equal coupling constant with the predator  $\alpha_1 = \alpha_2 = \alpha$ , it diverges. The scaling of the relative distance between the catching as it begins to diverge  $\alpha_1 \rightarrow \alpha_2$ , which to first order, reads

$$x_1(t) - x_2(t) \approx A(t - t^*) + \dots, \quad (22)$$

with the prefactor  $A$  scales in the limit  $\alpha_1 \rightarrow \alpha_2$  as  $\ln A \sim 1/(\alpha_1 - \alpha_2)$ . [17]

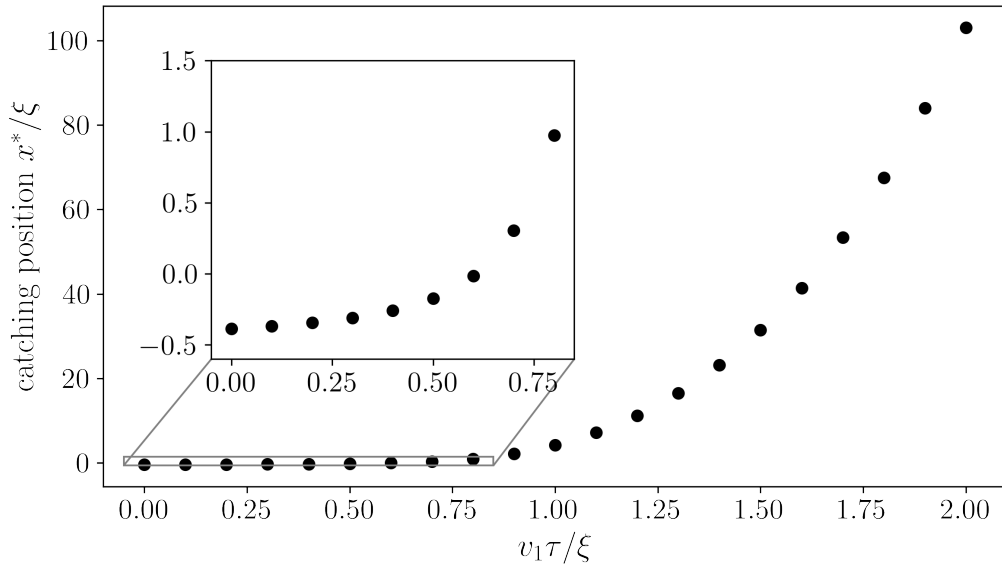


Figure 15: Increasing self-propulsion velocities, respectively to its catching position

Now, we have observed all conditions with different conditions of coupling constant values. Finally, in Fig.(15) we can see the catching position in a wide range of self-propulsion velocity of the prey, except that the coupling constant of the prey is smaller than the predator. This ensures that no prey is able to escape. With smaller self-propulsion velocity, it is clear that the catching happens before the prey is able to go over the summit, and some of them are smaller than the initial condition, so the prey is moving away from the summit. Gradually, when the velocity increases, the predator will take some time to catch the prey, and it will be caught after both the prey and the predator have overcome the barrier.

### 3.4 Regions

All the information from sections (3.2) and (3.3) are now plotted on a state diagram. Fig.(16) shows the catching regions of prey and predator through the coupling constants  $\alpha_1/\alpha_2$  respectively to their self-propulsion velocities  $v_1/v_2$ . We can see that the cases change depending on the self-propulsion velocity and coupling constant values, thus creating regions of catching and escape.

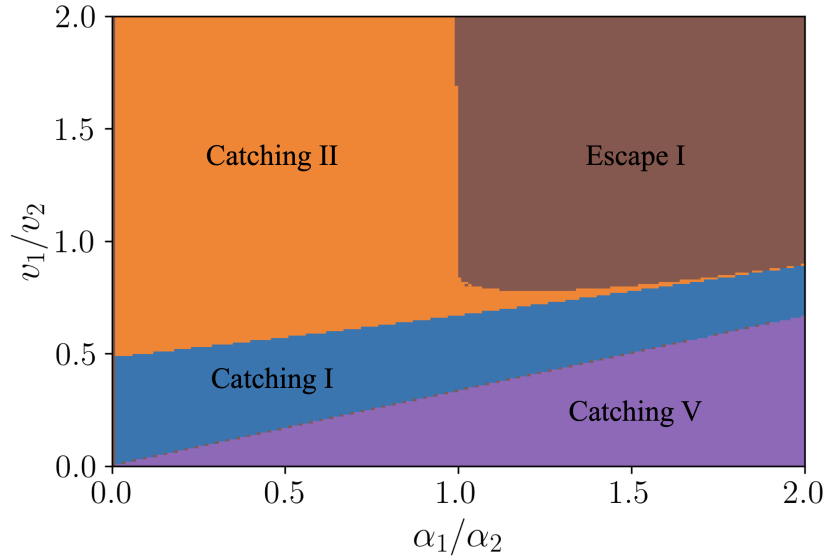


Figure 16: State diagram with initial conditions  $x_1(0) = -\xi/3$  and  $x_2(0) = -\xi/2$

## 4 Periodic predator-prey results

By evaluating the Eqs.(14)-(15) we can conclude that the speed of both predator and prey  $v_{1,2}$  must be greater than their respective coupling constants  $\alpha_{1,2}$  to the respective periodic potential barrier. If this condition were not satisfied, that is, if their velocity and their coupling constants were equal to or less than  $v_i \leq \alpha_i$ , neither of them would be able to cross the barrier and the algorithm needs a real-valued solution. Therefore, here we observe a catching within the parameter that  $v_1 > \alpha_1$  and  $v_2 > \alpha_2$ , where the predator will definitely catch the prey after the barrier. Both the prey and the predator have the initial conditions  $x_1(0) = \pi\xi/3$  and  $x_2(0) = \pi\xi/8$ .

### 4.1 Trajectory

In this section, Figs.(17a)-(17d) show the trajectories of the positions of the prey and the predator  $x/\xi$  respectively by time  $t$ . Because of the limits that were given to represent a circle between  $[0, 2\pi]$  in Eqs.(14)-(15), there are lines indicating that if the prey and predator's position  $x_{1,2}(t) > 2\pi$ , they will jump back to their original position, which is  $x_{1,2}(t) = 0$ . To simplify the observation, we have classified the occurrences in four possible parameters.

no.	parameters
1	$v_1 > v_2, a_1 < a_2$
2	$v_1 > v_2, a_1 > a_2$
3	$v_1 < v_2, a_1 < a_2$
4	$v_1 < v_2, a_1 > a_2$

Table 4: Possible catching parameters for periodic trajectories

In both Figs.(17a)-(17b), the prey is much faster than the predator  $v_1 > v_2$  and after few periods of looping the barrier, the predator catches the prey. Even when the prey's coupling constant  $\alpha_1$  is larger than the predator's  $\alpha_2$ , as shown in Fig.(17b), the catching also takes longer. However, in both Fig.(17c)-(17d), the predator is much faster than the prey  $v_2 > v_1$ . This results in a faster catching and the predator can directly catch the prey in the first period. This also occurs in Fig.(17c), where the predator has a smaller alpha than the prey.

The parameters  $v_{1,2}$  and  $\alpha_{1,2}$  are changed accordingly to the specific regions following the Table (4) to show at which time the predator catches the prey. If the predator catches the prey, they will meet at a specific time, and this event is marked by the black dot.

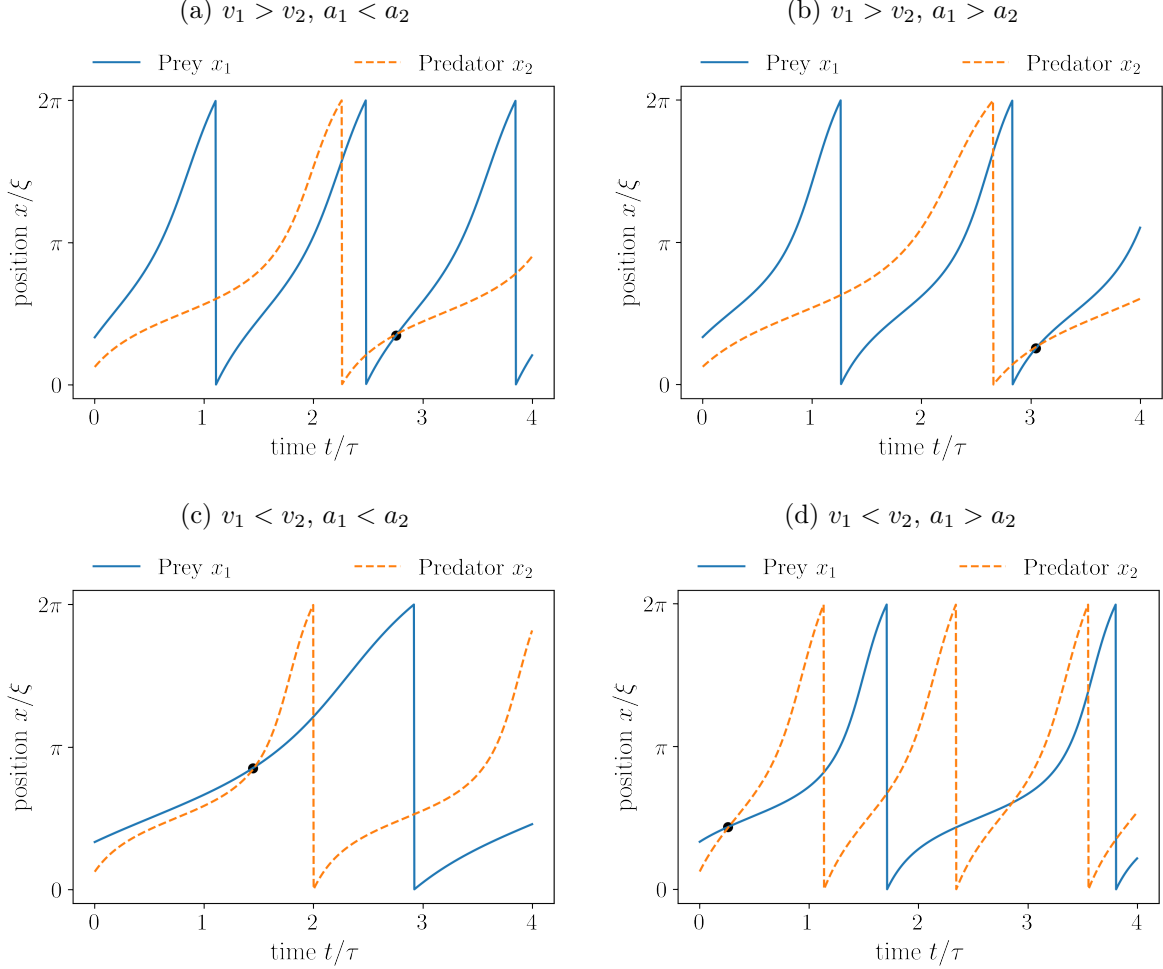


Figure 17: Periodic predator-prey positions with the condition  $x_1(0) = \pi\xi/3$  and  $x_2(0) = \pi\xi/8$ . The black dot marks the catching event.

## 4.2 Catching time

In the following section, we discuss the relation of the catching time  $t^*$  with the coupling constants  $\alpha_{1,2}$  and self-propulsion velocities  $v_{1,2}$  of the prey and the predator. This is determined by the method that is explained in Sec.(2.3.2). The Figs.(18)-(19) show the catching time  $t^*$  as a function of the prey's coupling constant  $\alpha_1$ . The velocity of the prey is here higher than that of the predator  $v_1 > v_2$ , but with a varying coupling constant of  $\alpha_1 = [1, 10]$ .

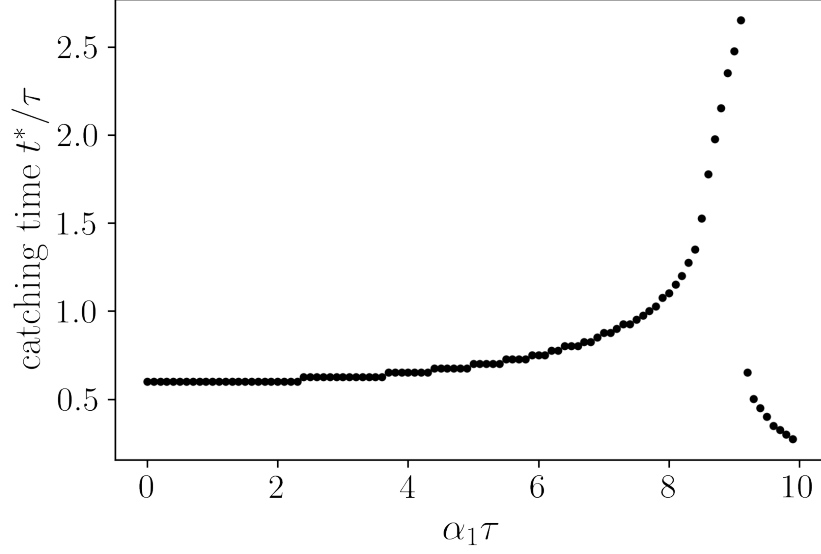


Figure 18: Catching time with initial conditions  $x_1(0) = \pi\xi/3$  and  $x_2(0) = \pi\xi/8$ , with increasing coupling constant of the prey  $\alpha_1 = [1, 10]$  and  $v_1 = 10$  and a fixated  $v_2 = 2$  and  $\alpha_2 = 1$ .

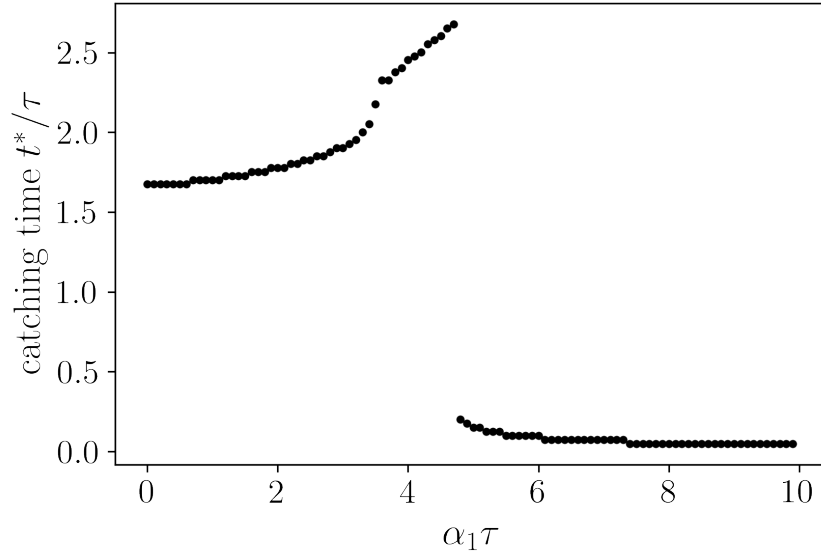


Figure 19: Catching time with initial conditions  $x_1(0) = \pi\xi/3$  and  $x_2(0) = \pi\xi/8$ , with increasing coupling constant of the prey  $\alpha_1 = [1, 10]$  and  $v_1 = 10$  and a fixated  $v_2 = 7$  and  $\alpha_2 = 1$ .

Both Figs.(18)-(19) show that there is a perturbed exponential growth of the catching time. When the prey's coupling constant increases, it also gradually increases the catching time needed. In Fig.(18), where the predator's self-propulsion velocity is much lower than the prey, there's a significant decrease jump of the catching time around  $\alpha_1 = 9$ . This jump also occurs in Fig.(19)



around  $\alpha_1 = 5$ , where the predator's self-propulsion velocity is close to the prey's self-propulsion velocity. After the jump, slowly the catching time also decreases.

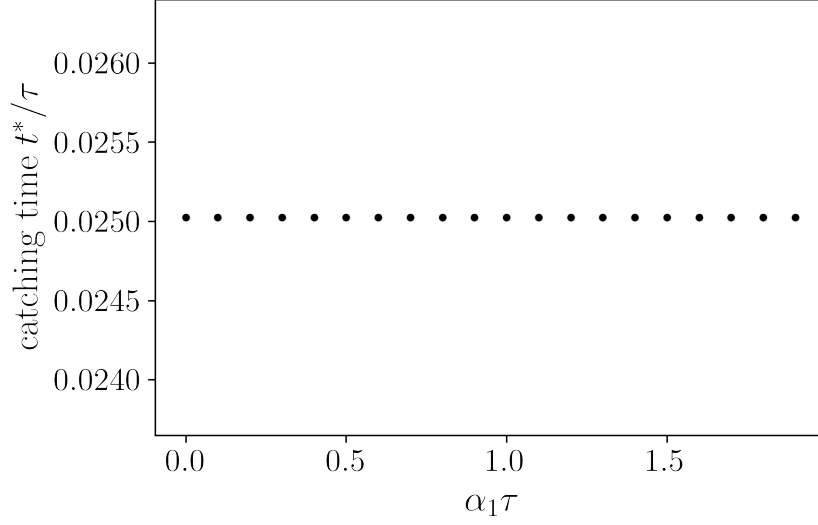


Figure 20: Catching time with initial conditions  $x_1(0) = \pi\xi/3$  and  $x_2(0) = \pi\xi/8$ , with increasing coupling constant of the prey  $\alpha_1 = [1, 10]$  and  $v_1 = 2$  and a fixated  $v_2 = 10$  and  $\alpha_2 = 1$ .

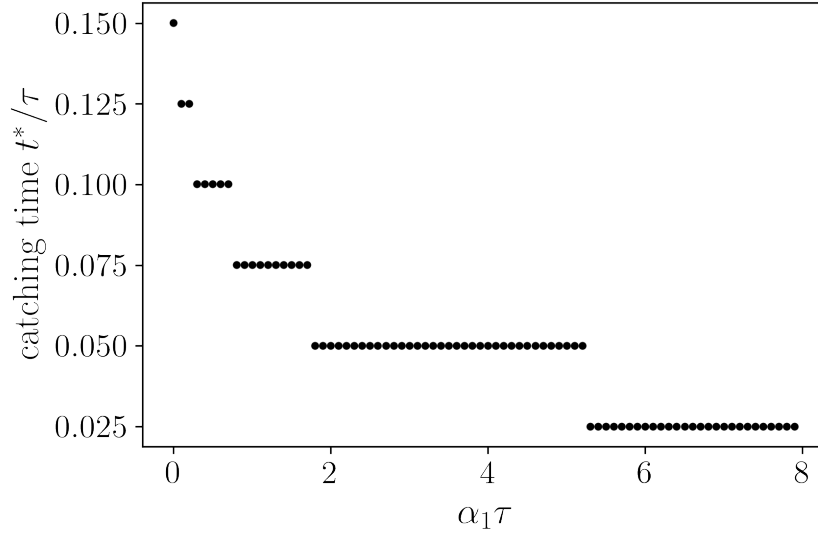


Figure 21: Catching time with initial conditions  $x_1(0) = \pi\xi/3$  and  $x_2(0) = \pi\xi/8$ , with increasing coupling constant of the prey  $\alpha_1 = [1, 10]$  and  $v_1 = 8$  and a fixated  $v_2 = 10$  and  $\alpha_2 = 1$ .

The Figs.(20)-(21) show the catching time  $t^*$  as a function of the prey's coupling constant  $\alpha_1$  as well, but here the velocity of the prey is lower than that of the predator  $v_1 < v_2$  and also with a varying coupling constant of  $\alpha_1 = [1, 10]$ . However, as explain in the beginning of Sec.(4),

catching can only occur when the prey's velocity is bigger than its coupling constant  $v_1 > \alpha_1$ , therefore in Fig.(21), there's no value beyond  $v_1 = \alpha_1 = 2$  and the same is for Fig.(21) beyond  $v_1 = \alpha_1 = 8$ . Fig.(20 shows that the catching time stayed consistent until  $\alpha_1 = 2$ . However, Fig.(21 shows an interesting staircase pattern of catching time, as it decreases as the coupling constant of the prey increases. This staircase pattern also happens in Fig.(18)-(19 when we look at the dots closely.

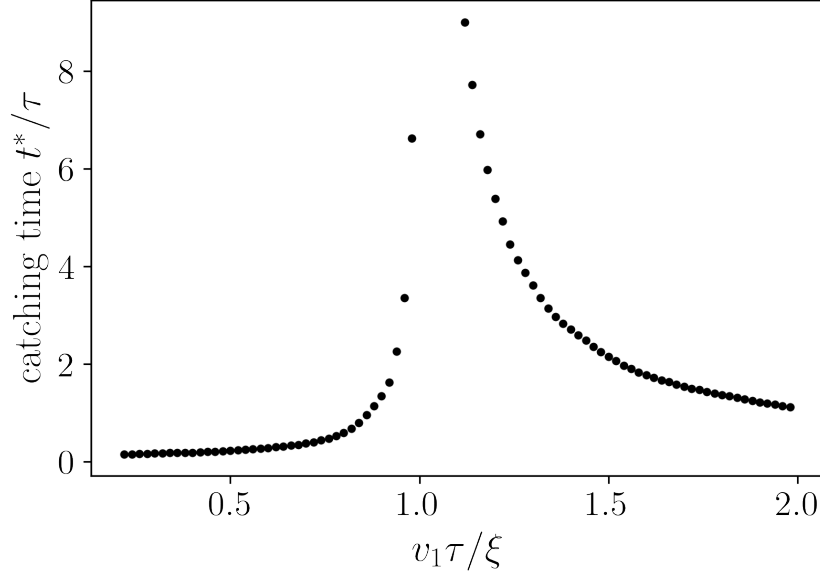


Figure 22: Catching time with initial conditions  $x_1(0) = \pi\xi/3$  and  $x_2(0) = \pi\xi/8$ , with increasing self-propulsion velocity of the prey  $v_1$  between  $[0, 10]$  and  $\alpha_1 = 1$  and a fixated  $v_2 = 5$  and  $\alpha_2 = 1$ .

The Fig.(22) shows catching time  $t^*$  as a function of the prey's self-propulsion velocity  $v_1$ . There is also a discontinuity of the catching time. It increases exponentially slowly at first, but when it reaches a similar speed as the predator, the catching time jumps higher and higher. This phenomenon is presumably due to the fact that the effective average velocity of both prey and predator are almost equal  $\overline{v_1}/\overline{v_2} \approx 1$ , since here we also take into account that the coupling constant has also influenced the outcome of the catching. Theoretically, there can be no catching around this value, since the prey and the predator will circle around the potential at approximately the same speed. When the ratio of the prey's and the predator's velocity increases  $v_1/v_2 > 1$ , catching can occur. After the jump, there is an exponential decrease, which shows that the catching time decreases when the prey is much faster because it loops back to zero after reaching  $2\pi$ , which means it will clash with the predator and then catching occurs.

### 4.3 Catching revolutions

We can now plot a function diagram of two variables based on the information from the Sec.(4.2) and use the method explained in Sec.(2.3.2) to plot the following figures. Figs.(23)-(24) show the catching revolutions of the prey and the predator through their coupling constants  $\alpha_1/\alpha_2$ , respectively to their self-propulsion velocities  $\alpha_1/\alpha_2$ . The number of revolutions changes depending on the self-propulsion speed and the coupling constants.

The number of revolutions required for the predator to catch the prey is shown in the Figs.(23)-(24). The dark blue region below the yellow line represents fast catching, because the prey is slower than the predator and the predator catches it before the prey can complete a full cycle. However, when the self-propulsion velocity of the prey and the predator reaches approximately the same, and considering the influence of the coupling constants, they reach an effective average velocity where  $\overline{v_1}/\overline{v_2} \approx 1$ . This means that, theoretically, catching cannot occur and the prey and the predator will always circle the boundary for an indefinite period of time and there is no clear definition of escape. Since it is impossible to achieve infinite precision with a finite number, we have chosen a reasonably large time interval in our algorithm to identify all possible catching. We identify all instances with catching time larger than  $t/\tau = 35$  with infinite, which is shown by the yellow line.

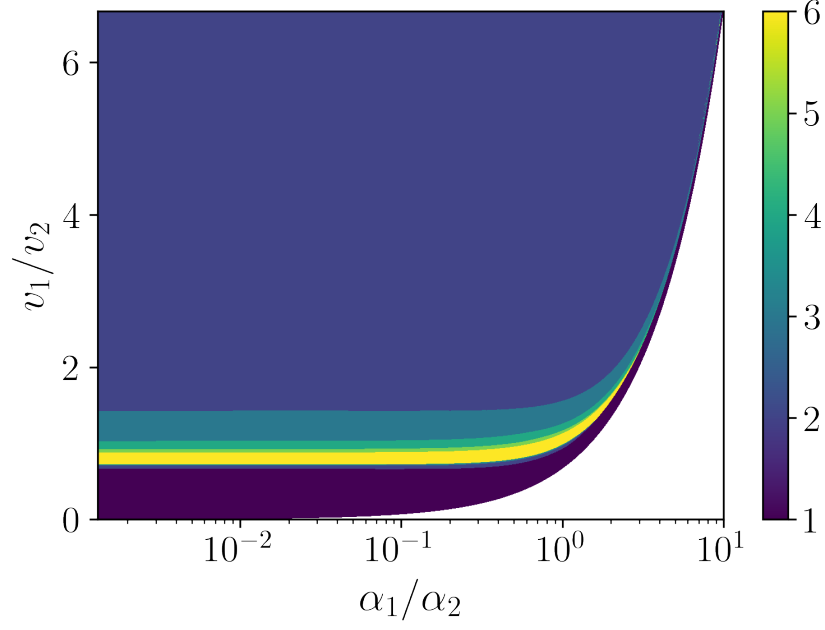


Figure 23: State diagram with initial conditions  $x_1(0) = \pi\xi/3$  and  $x_2(0) = \pi\xi/8$ , parameters for the prey varies in range  $v_1, \alpha_1 = [1, 10]$  of 10/2000 intervals and the predator  $v_2 = 1.5, \alpha_2 = 1$

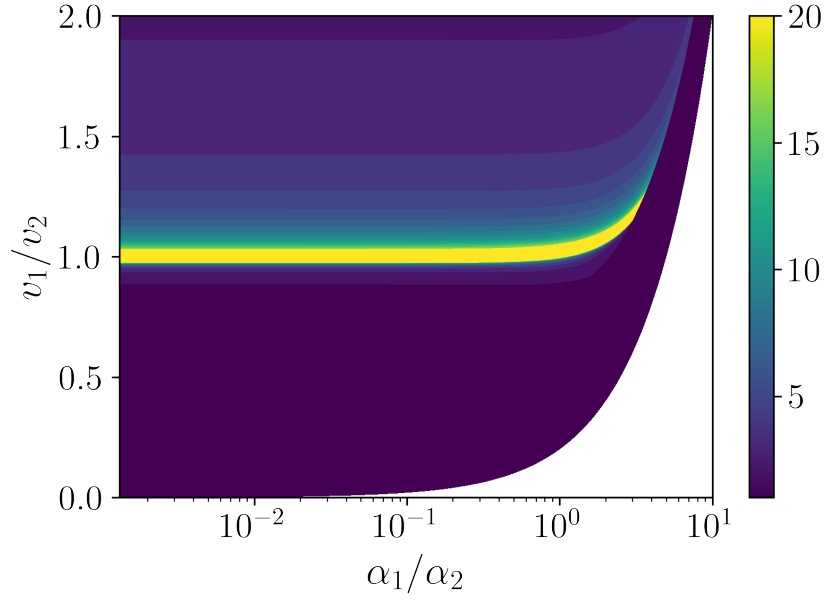


Figure 24: State diagram with initial conditions  $x_1(0) = \pi\xi/3$  and  $x_2(0) = \pi\xi/8$ , parameters for the prey varies in range  $v_1, \alpha_1 = [1, 10]$  of 10/2000 intervals and the predator  $v_2 = 5, \alpha_2 = 1$

When the prey's average speed exceeds the predator's  $v_1 > v_2$ , which is shown in the Fig.(23)-(24) along the vertical axis, there's a slowly changing colour gradient from yellow back

to blue and finally to a darker blue. This is presumably because the prey has circled around the boundary and is returning to the starting point and colliding with the predator, which may or may not have completed its first full loop or may have completed fewer loops than the prey.

If we look at the right-hand side of Figs.(23)-(24), we see not only an increase in the self-propulsion velocity along the vertical axis, but also an increasing value of the coupling constant along the horizontal axis. As the coupling constant slowly increases, it becomes much more difficult for both the prey and the predator to cross the potential boundary and both of them move more slowly. Only by increasing the speed of both prey and predator can catching occur again. The dark blue line that follows the pinching means that as long as the prey is faster than the predator, it does not matter if they both have larger coupling constants, catching can still occur. This is shown by a "pinching" of the colours in both figures.

"Pinching" also occurs for the white region in Figs.(23)-(24). This is the region where the coupling constants of both prey and predator are greater than the self-propulsion velocity  $a_{1,2} > v_{1,2}$ , where both the prey and the predator cannot cross the barrier. Theoretically, even then, catching can still happen between the prey and the predator, as in the example of the wolf and the deer. If both were trapped in the barrier, the wolf would eventually catch the deer. However, because of the model of Eqs.(14)-(15), the algorithm cannot give results and needs real-valued solutions.

## 5 Summary and Outlook

The survival of prey depends not only on its coupling constants and self-propulsion velocity but also on the complexity of its environment. In this thesis, we presented a one-dimensional model for each prey and predator in the presence of a potential barrier and classified the characteristic states for both catching and escape. We determined the catching time and catching position and explored the occurrence of different catching and escape states depending on the self-propulsion velocity and coupling constant to the barrier. With this knowledge, we created a state diagram that shows us the complexity that defines the different cases of catching and escape for the case of parabolic potential. For the periodic potential, we created a function diagram of the self-propulsion velocity and the coupling constant, that shows the number of revolutions needed for a catching to occur.

The behaviour of the prey and predator is highly dependent on the type of potential barrier, as well as their speed and coupling constant relative to the barrier. In the case of a parabolic potential barrier, catching can occur even if neither the prey nor predator summit the barrier, whereas in a periodic boundary condition, because of the complexity of the algorithm that we have, catching is only observed if they are able to overcome the barrier. It also takes more than one revolution for the predator to catch the prey, depending on their speed and coupling constants. Because of the periodic boundary, they are trapped within and escape is undefined, therefore even after a long time there is a possibility they don't catch each other at all when they reach an equal of the average effective velocity.

The predator-prey model under the parabolic boundary condition has been studied by introducing fluctuations to the ideal model. Furthermore, the classification of predators and prey based on their swimming strategies (pushers or pullers) has been shown to influence their chances of catching or escaping. [17] Further study is needed to understand the behaviour of the prey and the predator when they do not overcome the periodic barrier, while also adding the impact of swimming strategies and fluctuations on predator-prey dynamics in the periodic boundary condition. This is to check if our idealised model consistent with realistic conditions. One possible experiment to understand this model realistically involves is to study oil droplets chasing each other, as explored in the work of [11] and to add a physical boundary that replicates the periodic boundary introduced in the thesis.

Overall, these results highlight the importance of carefully considering the specific parameters of the system when analysing predator-prey dynamics in different potential landscapes. This motivates further exploration of different potential landscapes to gain deeper insights into the behaviour of prey and predator under varying conditions. Moreover, introducing multiple prey into the model and or incorporating the possibility of reproduction [18] in either the prey or predator can significantly alter the outcome. These additional factors contribute to the complexity of the predator-prey interaction and merit further investigation to fully understand their impact.

## 6 Bibliography

- [1] L. A. Twardochleb, T. C. Treacle, and P. L. Zarnetske, “Foraging strategy mediates ectotherm predator-prey responses to climate warming,” Ecology, vol. 101, no. 11, p. e03146, 2020.
- [2] C. K. Ghalambor, D. N. Reznick, and J. A. Walker, “Constraints on adaptive evolution: The functional trade-off between reproduction and fast-start swimming performance in the trinidadian guppy (*poecilia reticulata*),” Am. Nat., vol. 164, no. 1, pp. 38–50, 2004.
- [3] G. Volpe and G. Volpe, “The topography of the environment alters the optimal search strategy for active particles,” Proc. Natl. Acad. Sci. U.S.A., vol. 114, no. 43, pp. 11350–11355, 2017.
- [4] R. Garcia, F. Moss, A. Nihongi, J. R. Strickler, S. Göller, U. Erdmann, L. Schimansky-Geier, and I. M. Sokolov, “Optimal foraging by zooplankton within patches: The case of daphnia,” Math. Biosci., vol. 207, no. 2, pp. 165–188, 2007.
- [5] J. D. J. Clare, B. Zuckerberg, N. Liu, J. L. Stenglein, T. R. V. Deelen, J. N. Pauli, and P. A. Townsend, “A phenology of fear: Investigating scale and seasonality in predator-prey games between wolves and white-tailed deer,” Ecology, p. e4019, 2023.
- [6] M. Hebblewhite and E. H. Merrill, “Trade-offs between predation risk and forage differ between migrant strategies in a migratory ungulate,” Ecology, vol. 90, no. 12, pp. 3445–3454, 2009.
- [7] J. Wu and P. Zha, “Preventive, mitigating and treatment strategies for containing or ending the COVID-19 pandemic,” Preprints, 2020.
- [8] A. Nsamela, P. Sharan, A. Garcia-Zintzun, S. Heckel, P. Chattopadhyay, L. Wang, M. Wittmann, T. Gemming, J. Saenz, and J. Simmchen, “Effect of viscosity on microswimmers: A comparative study,” ChemNanoMat, vol. 7, no. 9, pp. 1042–1050, 2021.
- [9] G. Volpe, I. Buttinoni, D. Vogt, H.-J. Kümmerer, and C. Bechinger, “Microswimmers in patterned environments,” Soft Matter, vol. 7, no. 19, p. 8810, 2011.
- [10] C. Jin, C. Krüger, and C. C. Maass, “Chemotaxis and autochemotaxis of self-propelling droplet swimmers,” Proc. Natl. Acad. Sci. U.S.A., vol. 114, no. 20, pp. 5089–5094, 2017.



- [11] C. H. Meredith, P. G. Moerman, J. Groenewold, Y. J. Chiu, W. K. Kegel, A. van Blaaderen, and L. D. Zarzar, “Predator–prey interactions between droplets driven by non-reciprocal oil exchange,” Nat. Chem., vol. 12, no. 12, pp. 1136–1142, 2020.
- [12] E. M. Purcell, “Life at low reynolds number,” Am. J. Phys., vol. 45, no. 1, pp. 3–11, 1977.
- [13] J. P. Brody, P. Yager, R. E. Goldstein, and R. H. Austin, “Biotechnology at low reynolds numbers,” Biophys. J., vol. 71, no. 6, pp. 3430–3441, 1996.
- [14] E. Lauga and T. R. Powers, “The hydrodynamics of swimming microorganisms,” Rep. Prog. Phys., vol. 72, no. 9, p. 096601, 2009.
- [15] T. R. Scavo and J. B. Thoo, “On the geometry of halley's method,” Am. Math. Mon., vol. 102, no. 5, p. 417, 1995.
- [16] G. Alefeld, “On the convergence of halley's method,” Am. Math. Mon., vol. 88, no. 7, p. 530, 1981.
- [17] F. J. Schwarzendahl and H. Löwen, “Barrier-mediated predator-prey dynamics,” EPL, vol. 134, no. 4, p. 48005, 2021.
- [18] D. Breoni, F. J. Schwarzendahl, R. Blossey, and H. Löwen, “A one-dimensional three-state run-and-tumble model with a ‘cell cycle’,” Eur. Phys. J. E Soft Matter, vol. 45, no. 10, p. 83, 2022.